Boundary-Layer Meteorology (2023) 189:281–304
https://doi.org/10.1007/s10546-023-00840-y

RESEARCH ARTICLE

The Arctic Fjord Breeze: Characteristics of a Combined Sea Breeze and Valley Wind in a Svalbard Fjord Valley

Matthias Henkies[1,2] · Knut Vilhelm Høyland[2] · Aleksey Shestov[1] · Christiane Duscha[3] · Anna Sjöblom[1]

Received: 3 July 2023 / Accepted: 30 October 2023 / Published online: 8 December 2023
© The Author(s) 2023

Abstract
Thermally-driven circulations are a frequent meteorological phenomenon in complex Arctic terrain, but the Arctic fjord breeze, a combined sea-breeze and up-valley wind, has received little attention. A field campaign was conducted in the valley Adventdalen in Svalbard in summer 2022 using a Scanning Doppler Lidar and automatic weather stations. It is shown that a local up-valley circulation occurred frequently in this valley, and that it was driven by the temperature and pressure gradient between valley and fjord, i.e., a fjord breeze. The fjord breeze existed in both large-scale up-valley and down-valley winds. Its strength, extent and depth varied due to the diurnal cycle of solar irradiation as well as the interaction with large-scale winds. In contrast to typical lower-latitude breezes, the Arctic fjord breeze could persist over several days. The breeze was found to be relatively strong even under small horizontal temperature contrasts and opposing large-scale winds, possibly due to an increase in the thermal pressure gradient by the surrounding topography.

Keywords Arctic · Complex terrain · Scanning Doppler Lidar · Sea breeze · Valley wind

1 Introduction

Understanding weather and climate is a key challenge in the Arctic. One reason is that numerical weather prediction (NWP) models work less well in Polar regions due to sparse observations and model shortcomings (e.g., Jung et al. 2016). Another reason is the amplified global warming in the Arctic (e.g., Moritz et al. 2002; Miller et al. 2010; Serreze and Barry 2011; Previdi et al. 2021). Moreover, there is a potential for climate change mitigation by utilizing renewable energy in the Arctic, since today many Arctic settlements mostly rely on

✉ Matthias Henkies
matthiashe@unis.no

1 Department of Arctic Technology, The University Centre in Svalbard, 9171 Longyearbyen, Norway

2 Department of Civil and Environmental Engineering, Norwegian University of Science and Technology, 7491 Trondheim, Norway

3 Geophysical Institute, Bergen Offshore Wind Center and Bjerknes Centre for Climate Research, University of Bergen, 5020 Bergen, Norway

fossil fuels as their primary energy source (de Witt et al. 2021). Wind power seems attractive as it is abundant throughout the year, hence there is a need for better understanding of the local wind climate.

Many components of the wind climate are still poorly understood, especially when it comes to local features of the wind and how the specialties of the Arctic environment influence the wind climate. Therefore this study investigates summertime local wind circulations in the Arctic, such as valley winds and sea breezes, since these phenomena and their combination have been explored in other regions, especially due to their relevance to air pollution (e.g., Zhong et al. 2004) or cloud formation (e.g., Leopold 1949). Moreover, local winds are very relevant to considerations of wind energy due to the strong dependence of the wind power potential on the wind speed, the possible deflection of wind by the terrain, or mountain-induced turbulence. Increased attention has been given to local winds lately, mostly to the sea breeze as it affects the wind profile and wind power potential in offshore and coastal areas (e.g., Mazon et al. 2015; Steele et al. 2015; Xia et al. 2022), but also to the local winds in Arctic areas such as Greenland (e.g., Radu et al. 2019).

Complex terrain, i.e., contrasts between land and sea, mountains, valleys, glaciers, and plains, is abundant not only in the Arctic, but in many places around the world. Complex-terrain winds can be divided into dynamically-driven winds and thermally-driven winds (e.g., Whiteman and Doran 1993). Dynamically-driven winds include blocking, funnelling or deflection of the large-scale flow by mountain ranges (e.g., Zardi and Whiteman 2013) as well as acceleration of flow in the lee of mountains in down-slope windstorms (e.g., Richner and Hächler 2013).

Thermally-driven winds arise due to local temperature gradients and usually reverse their direction twice a day along with a shift in the vertical temperature gradient. Winds occur on mountain slopes (up-slope during daytime), or along-valley. In addition to the possible inclination of the valley bottom, the volume of air per flat ground area is reduced in a valley compared to a plain or broader valley, making the heating or cooling more efficient in a narrow valley, i.e., topographic amplification (e.g., Zardi and Whiteman 2013). Additionally, the air in a valley is prevented from mixing efficiently with the surrounding air, which reduces the heating or cooling. The temperature difference hence leads to up-valley winds during daytime and down-valley winds during night-time, extending vertically over several hundred metres.

Thermally-driven winds can also develop at the interface of a large water body and land, i.e., sea/lake breeze (on-shore during daytime), and land breeze (off-shore at nighttime). Sea/lake breezes and mountainous-terrain winds can couple, known as an extended sea/lake breeze (e.g., Mahrer and Pielke 1977; Kondo 1990). In specific places, if the adjacent sea is cold enough to inhibit the diurnal temperature and wind reversal in summer, up-valley winds can persist over night, e.g., in California's Central Valley (e.g., Zhong et al. 2004) or Chile's Elqui Valley (Kalthoff et al. 2002; Khodayar et al. 2008).

Studies of thermally-driven winds in Polar regions have mostly concentrated on wintertime winds such as the large-scale katabatic winds of Antarctica (e.g., Van Den Broeke and Van Lipzig 2003; Parish and Bromwich 2007) and Greenland (e.g., Bromwich et al. 1996) or local winds and the boundary layer over glaciers (e.g., Claremar et al. 2012; Esau and Repina 2012), valleys (e.g., Mayer et al. 2012; Valkonen et al. 2020) and fjords (e.g., Kilpeläinen et al. 2011; Mäkiranta et al. 2011; Vihma et al. 2011; Kilpeläinen et al. 2012; Schön et al. 2022) in Svalbard (Fig. 1a). The effect of these winds on the environment has also been addressed (e.g Kitowska and Petelski 2021; Cisek et al. 2017). Further, several studies have investigated complex-terrain dynamically-driven winds in Svalbard (e.g., Skeie and Grønås 2000; Sandvik and Furevik 2002; Barstad and Adakudlu 2011; Shestakova et al. 2022).

However, there are few reports about summertime thermally-driven winds in the Arctic. Kozo (1982) found a sea breeze at the (flat-part) north coast of Alaska, while meso-scale simulations suggest that parts of the North-Alaskan sea breeze also extend to the adjacent mountain ranges (Zhang et al. 2016). In Greenland the warm tundra is found to accelerate the katabatic wind from the ice-sheet in summer (Oerlemans and Vugts 1993; Gallée and Duynkerke 1997). In contrast, a combined sea breeze and valley wind has been found in Antarctica's dry valleys, counteracting the katabatic winds from the ice-sheet there (McKendry and Lewthwaite 1992; Doran et al. 2002; Nylen et al. 2004). In Svalbard, sea-breeze like circulations have been identified, e.g., in Ny-Ålesund (Beine et al. 2001) as well as Isfjorden, where the circulation could persist over several days in July (Grønås and Sandvik 1998). Idealized simulations confirm that it is possible for sea breezes north of 60°N to persist over several days in July because the sun does not, or only briefly, set (Grønås and Sandvik 1998). However, Kitowska et al. (2021) claim that the meso-scale circulations in Ny-Ålesund and Hornsund in Svalbard are not driven by a sea breeze, but rather mountain-induced eddies or, mostly, driven by a land breeze.

The Svalbard archipelago is therefore an ideal place to investigate Arctic summertime thermally-driven winds in more detail. Svalbard's largest island Spitsbergen lies at 77–80°N, which is why it has midnight sun during summer (from ca. 19 April to 24 August). In summer, most areas beside glaciers are snow free and can reach temperatures over 10 °C. Because of the complex terrain with mountains, fjords, and valleys (see Fig. 1b), the contribution of valley winds, besides sea breezes, has to be considered as well, which many studies have not addressed specifically so far.

Therefore, a study was performed in the fjord-valley Adventdalen (78°N) in central Spitsbergen (Fig. 1b). A combination of a sea breeze and valley wind, called a *fjord breeze* here, was investigated during a field campaign in the summer of 2022 (see Sect. 2). The results (Sect. 3) present the characteristics of the fjord breeze both through case studies, illustrating its thermal driver as well as diurnal variability and multi-day persistence, and an analysis of its vertical and spatial properties over two months. Finally the results are discussed and summarized in Sect. 4.

2 Data and Methods

2.1 Study Area

Measurements were conducted in Adventdalen, Svalbard, in July and August 2022 using a Scanning Doppler Lidar and temporary weather stations. They are complemented by permanent weather station and reanalysis data.

Adventdalen is a U-shaped valley in central Spitsbergen. It is connected to the fjord Adventfjorden (Fig. 1c). Together they stretch approximately 40 km from the large fjord Isfjorden in the west (W) to the east (E). The outer part of Adventdalen is characterised by a 3 km broad bottom. Adventdalen is curved so that the outer part and Adventfjorden align in a SE–NW (125/305°) direction. Adventdalen is surrounded by steep mountains on all sides, most of which have tops at 800 to 1100 m, and small tributary valleys, some of which are partially glaciated. South of outer Adventdalen, there are additionally plateaus of 400 to 600 m in altitude and a few kilometres in length. During the whole study period, Adventdalen was snow-free except for very few small, isolated patches.

Fig. 1 **a** Location of Svalbard; map data: Google, ©2022 Landsat / Copernicus Data SIO, NOAA, U.S. Navy, NGA, GEBCO IBCAO, U.S. Geological Survey. **b** Location of Spitsbergen, Adventdalen, and Isfjorden within the archipelago Svalbard; map data: TopoSvalbard ©2022 Norwegian Polar Institute (NPI). **c** Topographic map of Adventdalen with altitude lines every 100 m. The circles mark the position of automatic weather stations (see Sect. 2.1 and Table 1), the dashed line shows the valley axis. Map data: TopoSvalbard ©2022 NPI

2.2 Weather Stations

Figure 1 shows the locations of the automatic weather stations (AWSs); Table 1 their details.

The three AWSs V1, V3 and V4 are located approximately in line in the valley bottom; V1 south of the mouth of Adventfjorden, V3 at the tidally-variable (ca. 1 m vertically, few hundred metres horizontally) coast of Adventdalen (6 km from V1), V4 in Adventdalen (9 km from V1). V5 is on the hill Janssonhaugen at the bend between outer and inner Adventdalen (22 km from V1). V2 is also in Adventdalen, but elevated on a NNE slope between V1 and V3. Since V1, V2, V3, V4 and V5 lie in a line in Adventdalen, they can be used to determine

Table 1 Attributes of automatic weather stations (AWSs): Name, altitude (Alt.), type (perm. = permanent, temp. = temporary), measurement heights (in m above ground) and instruments of wind and temperature (Temp.), and time resolution

Short (long) name	Alt., type	Wind measurements	Temperature measurements	Time resolution
V1 (Svalbard Airport / Lufthavn)	28 m perm.	10.0 m	2.0 m	10 min
V2 (Platåberget Slope)	155 m temp.	3.8 m (YOUNG 8100 Ultrasonic Anemometer)	2.0 m (VAISALA HMP155)	1 min
V3 (Adventdalen Coast)	2 m temp.	2.0, 4.9 m (YOUNG Alpine Wind Monitor 05103-45)	2.0, 4.7 m (CAMPBELL S. CS215)	1 s
V4 (Old Auroral Station / Adventdalen)	7 m perm.	2.1, 10.1 m (YOUNG Alpine Wind Monitor 05103-45)	2.1, 9.1 m (YO. Platinum Temp. Probe 41342).	1 s
V5 (Janssonhaugen Vest)	250 m perm.	10.0 m	2.0 m	1 h
M1 (Platåberget)	450 m perm.	10.0 m	2.0 m	1 h
M2 (Nordenskiöldfjellet)	1041 m temp.	2.0, 4.4 m (YOUNG Wind Monitor 05103)	2.0, 4.0 m (CAMPBELL S. HygroVUE 10)	1 min

the horizontal extent of the fjord breeze, and through their different elevations the vertical extent. Moreover, V1 and V5 provided measurements of atmospheric pressure reduced to mean sea level (msl), allowing to calculate the local horizontal along-valley pressure gradient $\frac{\Delta p}{\Delta x}$.

The AWSs M1 and M2 lie above the valley (Fig. 1c). M1 is located on the plateau closest to the coast, M2 is on the flat, wide ridge of the mountain Nordenskiöldfjellet, 10 m below the peak. Due to their elevated position and in contrast to the other AWSs, M1 and M2 can be used to approximate the wind at higher altitudes, which is much less influenced by the fjord breeze.

The data of V1, V5, and M1, including their altitude, and the precipitation data at V4 come from MET Norway (2022). The data from V4 stem from The University Centre in Svalbard (2022) and the data of V2, V3, and M2 in Henkies et al. (2023b). The temporary installations have some data loss due to non-overlapping measurement periods, icing and instrument failure (M2), rain (on the sonic anemometer at V2), failed data recording (V3).

2.2.1 Stability and Turbulent Heat Fluxes

Since thermally-driven circulations are driven by the exchange of heat between the ground and the air, the stability in the surface layer was analyzed. Because measurements of temperature and wind were only available at two levels, the approach of Sjöblom (2014) was used to compute stability as well as turbulent heat fluxes. Stability was determined from the bulk Richardson number Ri_B:

$$Ri_B = \frac{g}{T_0} \frac{\Delta\Theta_v/\Delta z_\Theta}{(\Delta u/\Delta z_u)^2}, \tag{1}$$

which is an approximation of the Richardson number Ri, and where $g = 9.81\,\mathrm{m\,s^{-2}}$ is the gravitational acceleration, T_0 is the reference temperature of the air, $\Delta\Theta_v$ is the difference in virtual potential temperature between two height levels with difference Δz_Θ, and Δu the wind speed difference between two levels with difference Δz_u. Positive values indicate a stable stratification of air, negative ones unstable, and close to zero near-neutral conditions.

$-0.5 < Ri_B \leq 0.2$ can then be used to estimate the non-dimensional stability functions Φ_m and Φ_h, and the turbulent sensible heat flux H_S can be determined by the gradient method (for details see Sjöblom 2014):

$$H_S = -\rho c_p \frac{\kappa^2 \Delta u \Delta\Theta}{\Phi_m \Phi_h \ln(z_{u,2}/z_{u,1}) \ln(z_{\Theta,2}/z_{\Theta,1})}, \tag{2}$$

with ρ the air density ($\rho = 1.2\,\mathrm{kg\,m^{-3}}$ at 1000 hPa and 10 °C), $c_p = 1004\,\mathrm{J\,kg^{-1}\,K^{-1}}$ the isobaric heat capacity of air, $\kappa = 0.40$ the von Kármán constant, and $z_{u\backslash\Theta,1\backslash2}$ the heights of the measurements of u and potential temperature Θ, respectively. Positive values of H_S indicate upward heat fluxes, i.e., the ground is heating the air.

Following Sjöblom (2014), only measurements with $u \geq 2\,\mathrm{m\,s^{-1}}$, $\Delta u \geq 0.1\,\mathrm{m\,s^{-1}}$, and $\Delta\Theta \geq 0.1$ °C were used due to instrument uncertainties.

2.2.2 Radiation

A Kipp & Zonen CNR-1 Net Radiometer is located at V4. The radiometer measured the radiation components R_{up}^{SW}, R_{down}^{SW}, R_{up}^{LW}, R_{down}^{LW} (SW = shortwave, LW = longwave, up = upward, $down$ = downward). The net radiation R_{net}, which here is defined positive if directed downward, i.e., heating the ground, is defined as:

$$R_{net} = R_{net}^{SW} + R_{net}^{LW} = R_{down}^{SW} - R_{up}^{SW} + R_{down}^{LW} - R_{up}^{LW}. \tag{3}$$

The temperature of the ground T_G, assuming a black body, can be estimated as:

$$T_G = \left(\frac{R_{up}^{LW}}{\sigma} \right)^{1/4}, \tag{4}$$

where $\sigma = 5.67 \times 10^{-8}\,\mathrm{W\,m^{-2}\,K^{-4}}$ is the Stefan–Boltzmann constant.

2.3 Lidar Wind Profiling

A scanning Doppler Lidar (Windcube 100 S, Leosphere, Saclay, France; cf. Cheynet et al. 2021) was placed close to the weather mast at V4. The Lidar measured the profile of the three wind speed components by performing a 10-min Doppler Beam Swinging (DBS) scan for 10 min before every full hour, with the range gate set to 50 m. Wind was therefore measured only at elevations of 100 m and higher (with a resolution of 10 m using overlapping range gates). Only horizontal wind data with a carrier-to-noise ratio (cnr) of at least -27 and a quality index (output from Lidar) of at least 80 were considered valid. The vector-wise averaged wind data was valid if the average quality index was at least 15, with invalid data considered quality index 0. The Lidar was running between 7 July 1200 UTC and 23 August 1500 UTC, during which it not only faced minor power cuts, but, more importantly, periodically very low aerosol backscatter, which led to data loss. The data can be found in Henkies et al. (2023a).

Table 2 Direction ranges for classification of wind direction at V1, V4, V5

AWS	Up-valley	Down-valley	Cross-valley (from S)	Cross-valley (from N)
V1	230°–10°	70°–180°	180°–230°	10°–70°
V4	260°–350°	70°–170°	170°–260°	350°–70°
V5	200°–310°	40°–130°	130°–200°	350°–40°

2.4 Large-Scale Wind

The geostrophic wind, representing the large-scale flow (e.g. Whiteman and Doran 1993), was calculated from the 900-hPa geopotential of the reanalysis ERA5 (Hersbach et al. 2018):

$$u_g = -\frac{1}{f}\frac{\partial \Phi}{\partial y}, v_g = \frac{1}{f}\frac{\partial \Phi}{\partial x}, \tag{5}$$

where f is the Coriolis parameter ($f = 1.4 \times 10^{-4}\,\mathrm{s}^{-1}$ at 78° N), $\frac{\partial \Phi}{\partial x}$ and $\frac{\partial \Phi}{\partial y}$ are the geopotential gradients in x and y direction, respectively. The (spatially-)averaged geopotential gradient was obtained by least-squares fitting a plane to the geopotential field over a circle of 200 km radius centered around V1.

2.5 Fjord Breeze Identification Method

To allow for an automated identification of the fjord breeze, the wind direction at V1, V4, V5 was sorted into: *up-valley*, *down-valley*, *cross-valley (from S)*, *cross-valley (from N)*, or *lull* if the wind speed was below $1\,\mathrm{m\,s}^{-1}$. The corresponding direction ranges (Table 2) differ between the locations to account for the local topography.

For the wind to be considered as a fjord breeze, it was defined as arriving at one AWS when the direction was first up-valley, lasting the following hour. The fjord breeze was retreating from one AWS when the direction first was not up-valley for the following hour. However, the fjord breeze could not arrive at one AWS before it had arrived at the AWSs in the outer part of the valley.

The extent of the fjord breeze was categorized into *nowhere*, *over V1*, *over V4*, and *over V5*, depending at which AWSs it had arrived (and not yet retreated); e.g., if the fjord breeze had arrived at V4, the extent was *over V4*, which implies that it had also arrived at V1.

3 Results

3.1 Overview of the Local and Large-Scale Weather Situation

The temperature at V4, the valley bottom in the center of Adventdalen, varied between 0.0 and 16.5 °C during the campaign. There was precipitation (≥ 0.1 mm) on 23 out of 61 days with a total of 41.1 mm, which was mostly light rain or drizzle. It was warmer and drier during July than during August. The observations at V1 indicate that the weather was overall warmer compared to the climate period 1991–2020 (by 2.3 °C in July, 0.9 °C in August), as well as drier in July and wetter in August.

The large-scale wind situation is illustrated by the windrose of the 900-hPa geostrophic wind in Fig. 2. The direction ESE was most frequent although all directions were common.

Wind from S and N was least common, allowing the directions to be divided roughly in an E half and a W half. The wind direction distribution is similar at the mountain top M2 (Fig. 2), although the wind speeds at M2, especially from E, are higher than the geostrophic wind, and the directions are more E–W aligned than the rather ESE–WSW aligned geostrophic directions. This is likely due to the general E–W alignment of Adventdalen and the channelling it exerts on the geostrophic wind as well as the N–S alignment of the ridge at M2. Further, wind from the E half is much more frequent at M2 than in the geostrophic wind, which is mostly because of systematic data gaps at M2. These gaps occurred when atmospheric icing made reliable wind measurements impossible, with strong icing observed during wind from W. The geostrophic windrose would look very similar to M2 if only the valid timestamps of M2 were included (not shown).

In contrast to the relatively even direction distribution of the geostrophic wind, the windroses of the AWSs in the campaign area (Fig. 2) show strong effects of channelling with bimodal direction distributions due to the surrounding terrain: The direction maxima of the AWSs in the fjord and valley (V1, V2, V3, V4, V5) follow the direction of the local valley axis. V1, at the entry of the fjord valley, has a large fraction of up-valley winds (57 %) compared to down-valley winds (27 %). This fraction decreases gradually (44 % up- and 40 % down-valley at V4) towards V5, where down-valley winds are more frequent (50 %) than up-valley winds (35 %). M1, located on a plateau, has a wider direction distribution than the valley AWSs, but also shows a clear distinction between (roughly) up-valley and down-valley winds with approximately even shares.

A fjord breeze occurred on 55 of 62 days with a median daily maximum of 5.4 m s^{-1} at V4. As described in Sect. 2.5, the existence of a fjord breeze does not imply up-valley wind at every AWS in Adventdalen, which is further shown in Sect. 3.5.

3.2 A Fjord Breeze Example and Its Thermal Forcing

The existence of a local circulation independent of the large-scale wind, i.e., a fjord breeze, can easily be seen when the wind is up-valley in Adventdalen, but down-valley outside of Adventdalen and at higher altitudes. One case which illustrates this well, is 02 August: the wind was up-valley at the valley AWSs V1, V2, V3, and V4 for several hours, while the wind at the elevated AWSs V5, M1, M2, and the geostrophic wind were down-valley throughout the day (Fig. 3a, b). M1, M2 were very similar to the geostrophic wind, with down-valley wind directions, but with fluctuating wind speeds (not shown). This becomes even clearer from the evolution of the wind at different altitudes at V4 (Fig. 3c): the up-valley flow (blue) during the middle of the day extended up to 180 m and was topped by a layer of weak wind (< 1 m s^{-1}, pale colours) with down-valley winds (red) above.

This fjord breeze was present only at V1 all of the time, while it arrived and retreated at V3 and V4, switching wind direction. Before noon, it extended from V1 further towards Adventdalen and stretched over V3 (from 0900 UTC) and V4 (1000 UTC) (Fig. 3a). The fjord breeze did not reach V5. Instead, it shrunk in the evening, so that the wind turned down-valley again at V4 (1630 UTC) and V3 (1700 UTC). The wind shift at V2 is less clear because its location is partly within and partly above the up-valley flow, although the 20-min up-valley wind at V2 before the arrival at V3 could be the passage of the sea breeze front.

Such a shift in wind direction is similar to diurnal winds of lower latitudes. However, the situation is different in Adventdalen in summer. Due to the midnight sun, R_{net} is almost never negative. Therefore, the valley atmosphere is usually warmer than the fjord atmosphere, leading to a local pressure gradient, i.e., up-valley forcing, which drives the fjord breeze. Since

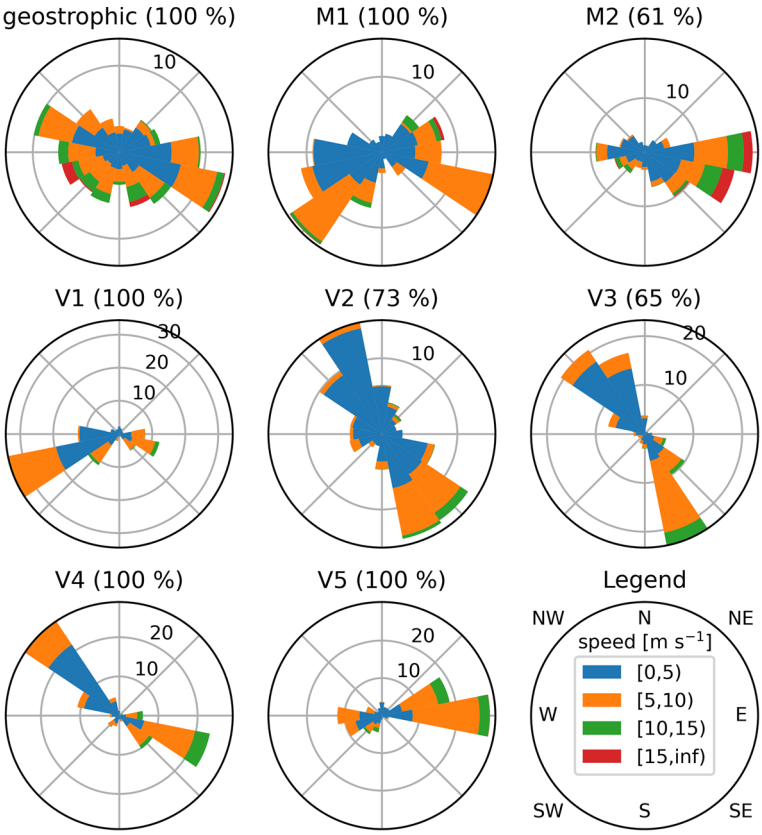

Fig. 2 Map of windroses at different AWS as well as the 900-hPa geostrophic wind in July and August 2022. The direction is where the wind comes from. The percentage is the data coverage. Rings show the relative frequency in percent per bin width

the thermal forcing seldom is down-valley, it is only the large-scale wind that can counteract the thermal up-valley forcing. Therefore, the fjord breeze is the result of both thermal forcing (up-valley) and forcing of the large-scale wind (down-valley). Because these forcings can be variable, the resulting fjord breeze can have different strengths or spatial extents depending on the strengths of the forcings.

On 02 August the forcing of the large-scale down-valley wind was nearly constant (Fig. 3a, b), while R_{net} increased in the morning and decreased in the evening (Fig. 4a). The evolution of temperatures at V3 and V4 (Fig. 4b) also shows that the air coming from the sea was colder than air over land. The temperatures at V3 and V4 decreased by ca. 1.5 °C when the fjord breeze reached the respective AWS, and increased again when the fjord breeze withdrew. It also shows that the air was warming during the passage of Adventdalen. Figure 4c indicates that Θ at the ground was always higher than at 2.1 m at V4. Moreover, Θ at 2.1 m (V4) was ca. 0.5 °C higher than at 9.1 m during the fjord breeze.

This temperature gradient makes the air at V4 unstable, as seen by the negative Ri_B in Fig. 4d. In contrast, the marine air at V3 is stable at the same time ($Ri_B > 0$). Many values are missing at V3 mostly due to very small $\Delta\Theta$ values. During down-valley wind the air at V4 was closer to neutral (mostly $-0.03 \leq Ri_B \leq 0.03$). H_S in Fig. 4a is therefore upward during

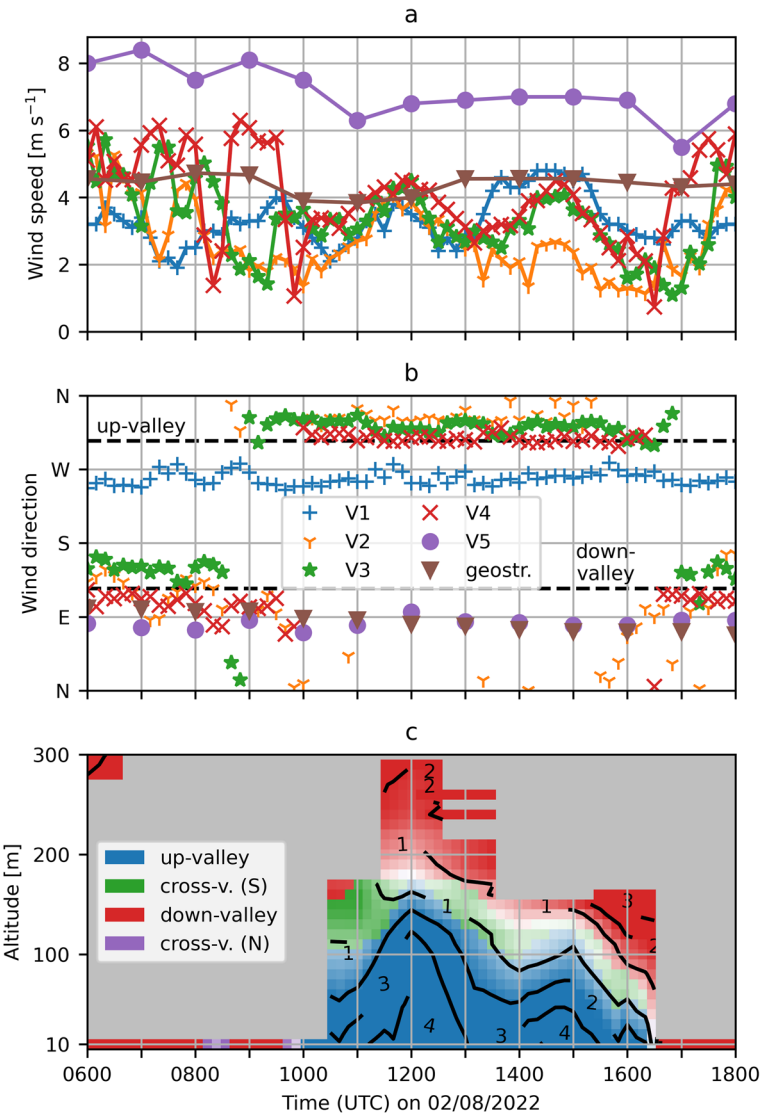

Fig. 3 Evolution of the fjord breeze on 02 August 2022. **a** Wind speed, **b** Wind direction at several AWSs (see Sect. 2.1 and Fig. 1c for a map) and the geostrophic wind. **c** Wind speed (contours of 1 m s^{-1}) and wind direction sector (colours) of the atmosphere above V4; values below 2 m s^{-1} are gradually whitened. The data in c is a combination of V4 AWS (at 10 m, every 10 min) and the Lidar at 100 m and higher (every hour). The Lidar data was interpolated in time for points at most 30 min away from the closest measurement, and the altitude range between 10 m and 100 m was interpolated between Lidar and AWS data. Missing data is grey

the fjord breeze, but around zero in down-valley wind. However, the ground-air temperature contrast suggests that H_S should have been upward all of the time.

That the heating of the ground actually led to a local pressure gradient can be seen in Fig. 4e. V1 always had higher msl pressure than V5 ($\frac{\Delta p}{\Delta x} > 0$), hence up-valley forcing. The forcing was strongest in the morning hours (up to 2.3 Pa km^{-1}) when the fjord breeze

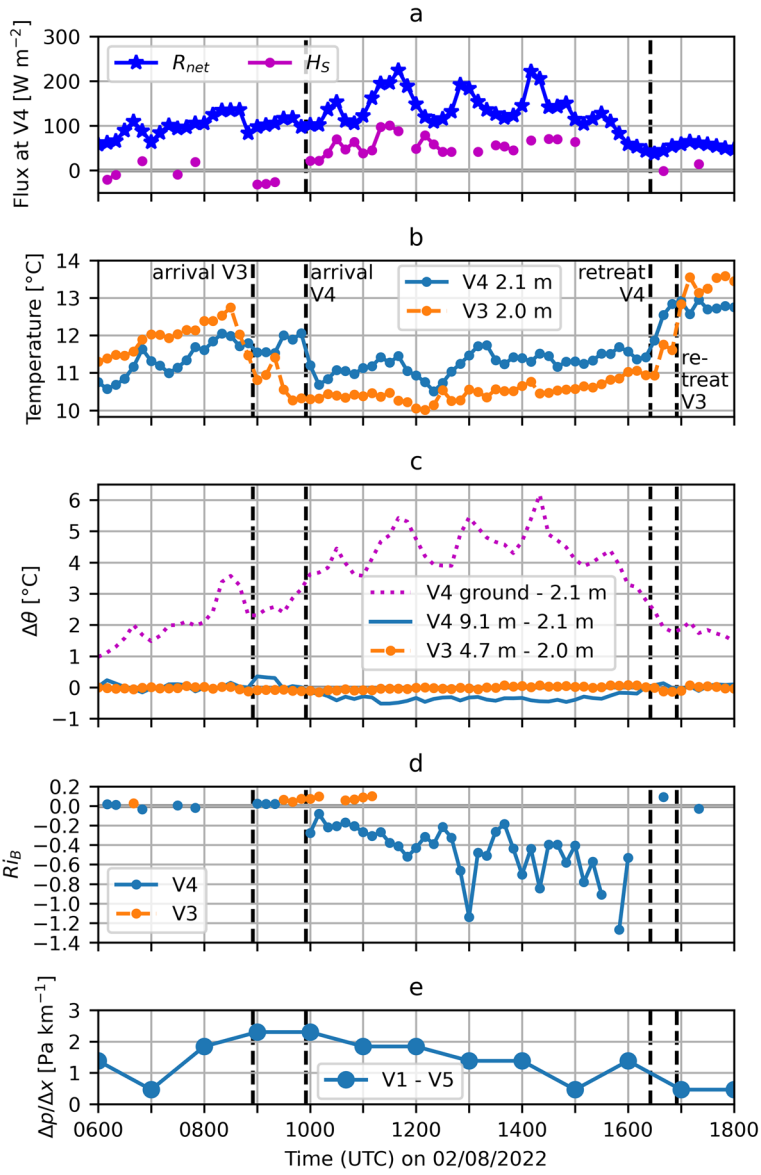

Fig. 4 The fjord breeze on 02 August 2022. **a** R_{net} (positive means downward) and H_S (positive means upward) at V4. **b** Air temperatures at V4 and V3. **c** Vertical temperature differences at V4 and V3. **d** Bulk Richardson Number at V4 and V3. **e** Gradient of msl pressure between V1 and V5; positive values mean that the msl pressure at V1 is higher than at V5. The vertical dashed lines mark the fjord breeze's arrival and retreat times at V3 and V4, as labelled in plot b

advanced. In comparison, the large-scale pressure gradient associated with the geostrophic wind of 4 m s^{-1} was much smaller. The absolute value was only 0.7 Pa km^{-1}, but the direction was not aligned with the valley axis, making the along-valley component even smaller.

3.3 Multi-Day Fjord Breeze

While the fjord breeze had a clear diurnal variability in the case shown above, it can persist over several days as well. This is illustrated by the case of 19 to 22 July. Figure 5a shows wind speed and direction at V4 at different altitudes over the period. Up-valley winds persisted from 19 July 2210 UTC to 22 July 0010 UTC at low levels (aside from 20 min of lull). The variable-depth, up to 300 m deep, up-valley wind layer was topped by a calm-wind layer and down-valley winds aloft, with the geostrophic wind 3 to 5 m s^{-1} from NE (cross-valley) to SE (down-valley) and the wind at V5 mostly from E (down-valley) up to 7 m s^{-1} (not shown). The up-valley wind can be identified clearly as a fjord breeze due to the difference in wind directions at lower and higher levels in Adventdalen.

Moreover, the forcing characteristics are similar to the example in Sect. 3.2. Both R_{net} and the ground-air temperature gradient were positive (heating the air) except for short periods of 2 h around midnight (Fig. 5b, c), which were not long enough to have an influence. As a result the msl pressure was higher at V1 than at V5 (forcing up-valley). In contrast to the case of 02 August (Sect. 3.2), the fjord breeze extended constantly over V4 because the large-scale wind was not able to counteract the fjord breeze forcing to the point where the fjord breeze would retreat from V4. However, the strength and the depth varied, with stronger and deeper up-valley wind around noon.

3.4 Fjord Breeze During Large-Scale Up-Valley Winds

While the fjord breeze in Adventdalen is easily discernible in large-scale down-valley winds, the identification is more challenging in large-scale up-valley winds. However, an example can be seen on 26 July. Figure 6 shows the key characteristics of the fjord breeze development, similar to Fig. 5. The wind direction at V4 (Fig. 6a) was up-valley in the lowest 600 m throughout the whole day except for very short periods with light cross-valley wind over a small altitude range. Above 600 m the wind was first from NE (cross-valley) and then turned to NW (up-valley), all of which is consistent with the geostrophic wind direction (from NE to N, 3–6 m s^{-1}) as well as measurements from the AWSs (not shown).

Because the wind was up-valley throughout the day, the fjord-breeze arrival and retreat times cannot be easily determined. However, there is a clear variability of wind speed at low levels; the speed is lowest in the morning and highest in the afternoon, with a maximum at 6 m s^{-1} around 100 m altitude. The depth of this low-level wind maximum, which is mostly topped by a weak-wind layer, is very variable, but generally smallest in the morning and largest in the afternoon. The weak-wind layer on top could be caused by a return flow. It allows for a rough division of the wind over different altitudes into a fjord-breeze driven part below and a large-scale-wind driven part above.

That the lower part is indeed a fjord breeze is substantiated by the observations of R_{net}, $\Delta\Theta$ and local pressure gradient (Fig. 6b–d), as discussed previously. They describe the thermal forcing leading to the fjord breeze buildup, which in this case was strongest from morning to noon. Moreover, such a diurnal variability is also discernible from the previous cases.

3.5 Spatial Variability

The previous sections have illustrated that up-valley wind in Adventdalen is often connected to the fjord breeze, especially when down-valley wind is found in the surroundings. It was shown that the fjord breeze in Adventdalen can persist over many days without diurnal

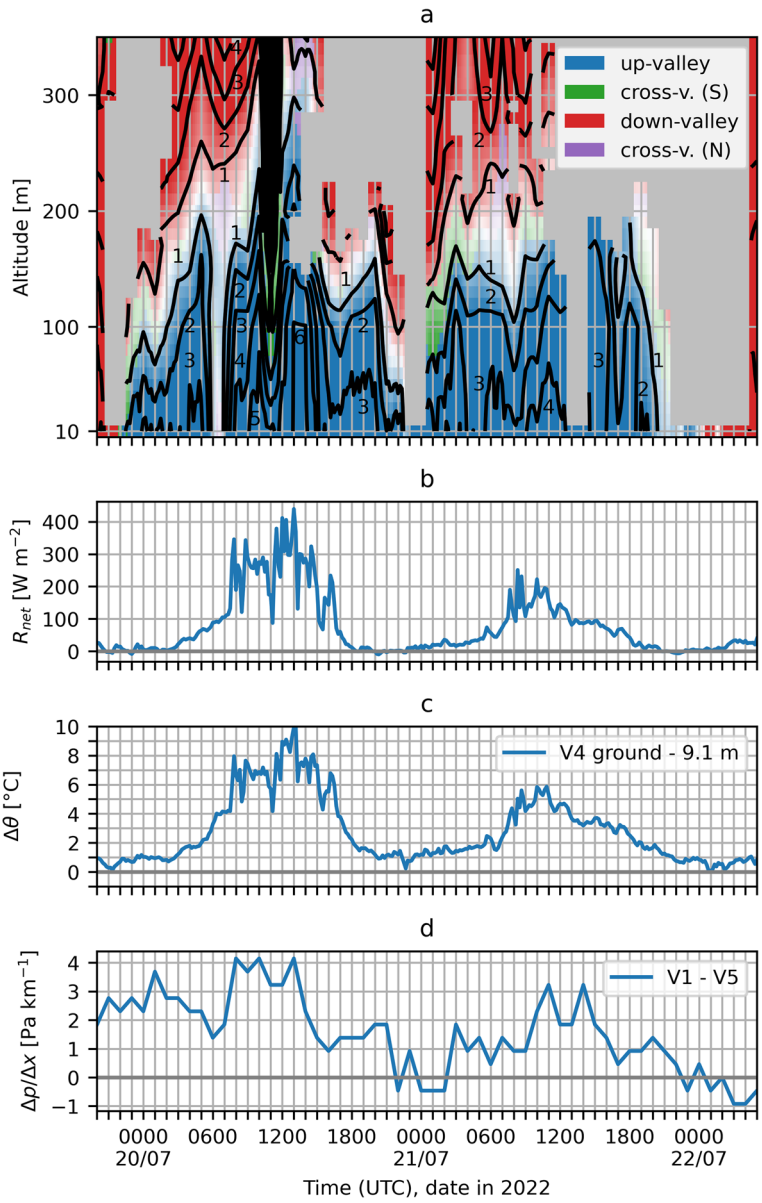

Fig. 5 Fjord breeze between 19 and 22 July at V4. **a** Wind speed and direction at different altitudes, see Fig. 3c. **b** R_{net}. **c** $\Delta\Theta$ **d** msl pressure gradient between V1 and V5

reversal although the fjord breeze is stronger during daytime than nighttime. However, these cases focused on the fjord breeze appearance at V4. On a more general scale, the fjord breeze influences the wind distribution throughout the whole fjord and valley.

Using the fjord breeze identification method (Sect. 2.5), the average fraction of time that the fjord breeze extended to a certain location could be determined. It was different for each station and variable throughout the day as Fig. 7a shows. Naturally, the fjord breeze reached

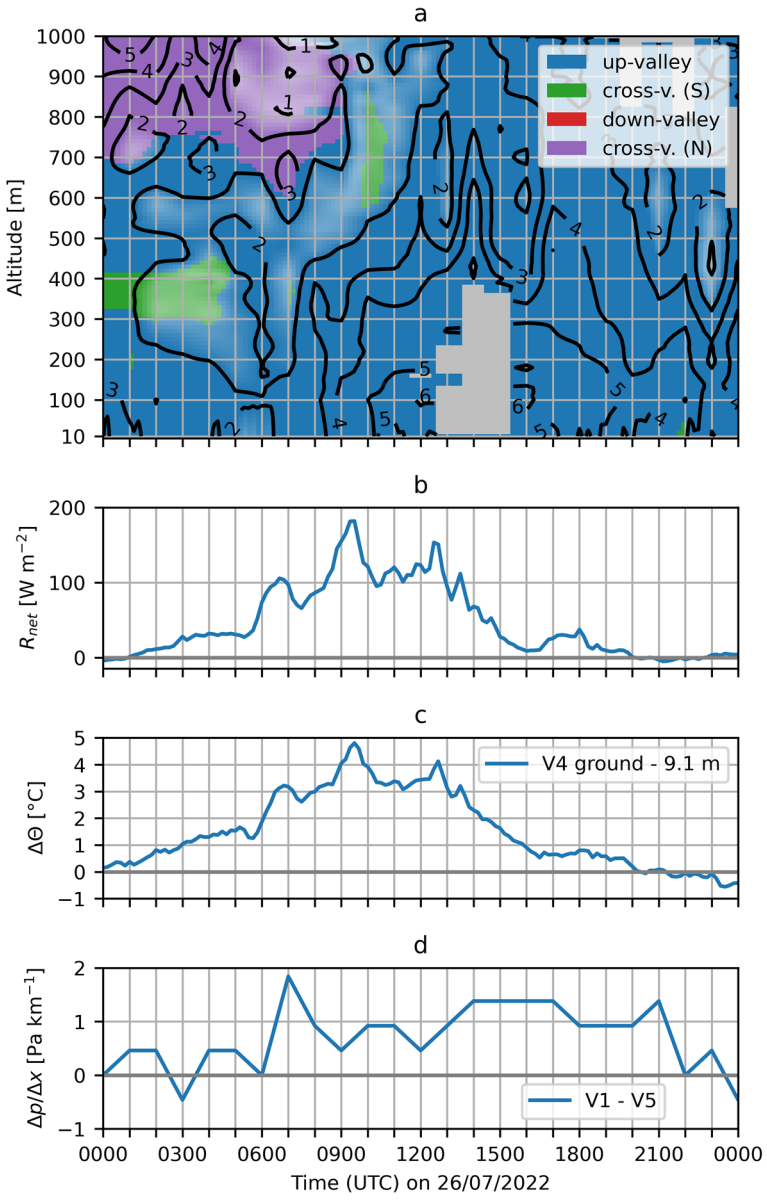

Fig. 6 Fjord breeze on 26 July 2022 at V4, for explanations see Fig. 5

V1 most often and V5 least. Short extents reaching only to V1 and absences were more common during night and early morning, while larger extents were more common in the afternoon or evening. The diurnal variation stresses the influence of the daily cycle on the fjord breeze development and that the fjord breeze is really driven by the local thermal forcing rather than large-scale up-valley wind.

The persistence, i.e. the duration between arrival and retreat of the fjord breeze at a certain location, is highly variable as Fig. 7b shows. The fjord breeze duration roughly varied between

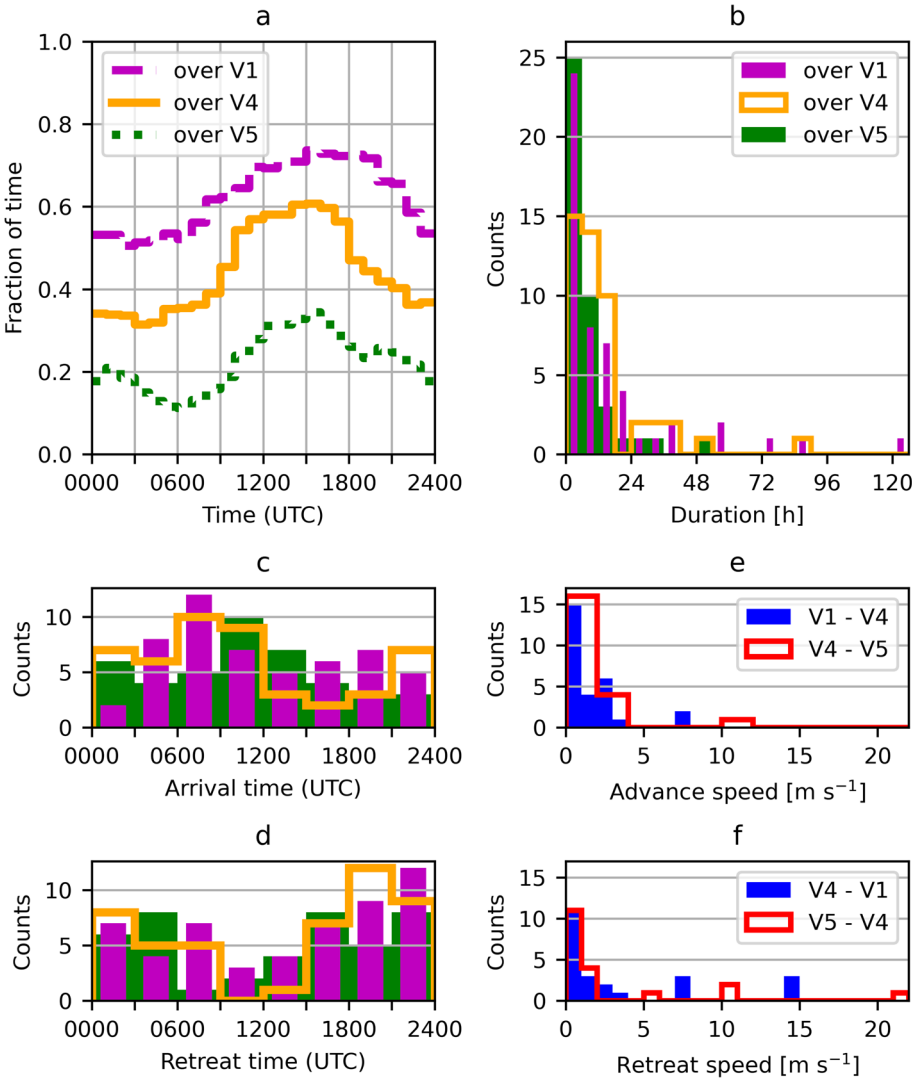

Fig. 7 Statistics of the fjord breeze in July and August 2022. **a** Frequency of the extent (classes) by daytime, bins of 1 h. **b** Duration, bins of 6 h. **c** Arrival times, bins of 3 h, same colours as b. **d** Retreat times, bins of 3 h, same colours as b. **e** Advance speeds, bins of 1 m s^{-1}. **f** Retreat speeds, bins of 1 m s^{-1}

1 h (minimum time, Sect. 2.5), and 125 h. Most often it persisted for only a few hours, but in 11 cases it lasted for more than 20 h, two of which have been illustrated in Secs. 3.3 and 3.4. Naturally, the maximum fjord breeze duration at V1 (5 d) is larger than at V4 (4 d), which again is larger than at V5 (3 d).

Not only did the fjord breeze last for several days, its arrival and retreat times were found at any time of the day, as seen in Fig. 7c, d, respectively. However, the fjord breeze arrival was most common from morning to noon, with the maximum at V1 earlier than at V4, which again was earlier than at V5. The retreat times of the fjord breeze follow the opposite pattern, with the majority of retreats in late afternoon to midnight. These daytime patterns fit well

to the fact that the extent was on average largest in the afternoon. In addition to the arrivals being most frequent from morning to noon, arrivals were also more common in late evening. This is possibly because Adventdalen is irradiated better when the sunlight is parallel to the valley axis (roughly at 09 and 21 UTC), while it is more shaded by the surrounding mountains during afternoon and night.

The distribution of advance and retreat speeds is shown in Fig. 7e, f. Some advances were very slow and took more than one day from one AWS to another. The medians of the advance speeds were 1.0 m s^{-1} (V1–V4 in 2.5 h) and 1.3 m s^{-1} (V4–V5 in 2.8 h), of the retreat speeds 1.3 m s^{-1} (V4–V1 in 1.8 h) and 0.9 m s^{-1} (V5–V4 in 4 h).

3.6 Vertical Extent

The sections above have shown that the fjord breeze in Adventdalen is often a few hundred metres deep, but can be highly variable from less than 100 m in strong large-scale counter wind to more than 1000 m in supporting large-scale wind. Besides, the fjord breeze tends to be deeper during advances than during retreats, since it usually reached V2 (at 150 m altitude) before V3 (in the valley bottom 2 km up-valley from V2) during advances, while it retreated from V2 earlier than from V3 (not shown).

Moreover, the fjord breeze led to stronger up-valley winds at low levels, while the wind speed was reduced in a layer above. The strength of the low-level wind speed increase can be seen in Fig. 8a. The average of the up-valley wind component (dotted) clearly shows the effect of the fjord breeze; it decreased from 3.2 m s^{-1} at 100 m to approximately zero at 400 m and above. However, the effect on the corresponding average (absolute) speed profile was smaller, decreasing from 3.7 m s^{-1} at 100 m to 2.5 m s^{-1} at 300 m, above which it increased again. This is because the wind at higher altitudes, especially above the height of the wind maximum, can have a different direction than the fjord breeze (up-valley). The 10-m wind speed (3.9 m s^{-1} absolute) was even slightly larger than at 100 m, indicating that the maximum wind speed may be found below 100 m.

Further, there was a wind speed decrease of 3.4 m s^{-1} between 100 m and 600 m for the down-valley regime (Fig. 8a), which was not driven by the fjord breeze. Instead, it is likely that the wind acceleration was induced by the down-slope descent from the mountain ranges east of Adventdalen, or a funnelling effect of Adventdalen's geometry in the lowest levels.

The fjord breeze was frequent (45 %) in July and August 2022 at V4, i.e., it influenced the average speed profile in Adventdalen to a high degree. Down-valley winds had a large contribution as well (40 %). Because both types of wind showed a decrease of wind with altitude, the total average wind profile had a similar speed decrease, from 100 m to 300 m, although less pronounced than for fjord-breeze or down-valley winds alone, and a speed increase from 600 m and upward (Fig. 8a). However, it must be considered that the average profiles in Fig. 8a have large amounts of missing data (Fig. 8b), especially down-valley, where the data coverage is less than 40 % in the lowest 300 m.

3.7 Influence of Radiative Fluxes

Usually, the daily amount of solar radiation, or even the amount before noon (Giovannini et al. 2015), determines whether an up-valley wind can develop. However, this is less relevant to Adventdalen's fjord breeze. The case studies showed that the fjord breeze could develop even when the daily maximum of R_{net} hardly exceeded 200 W m^{-2}.

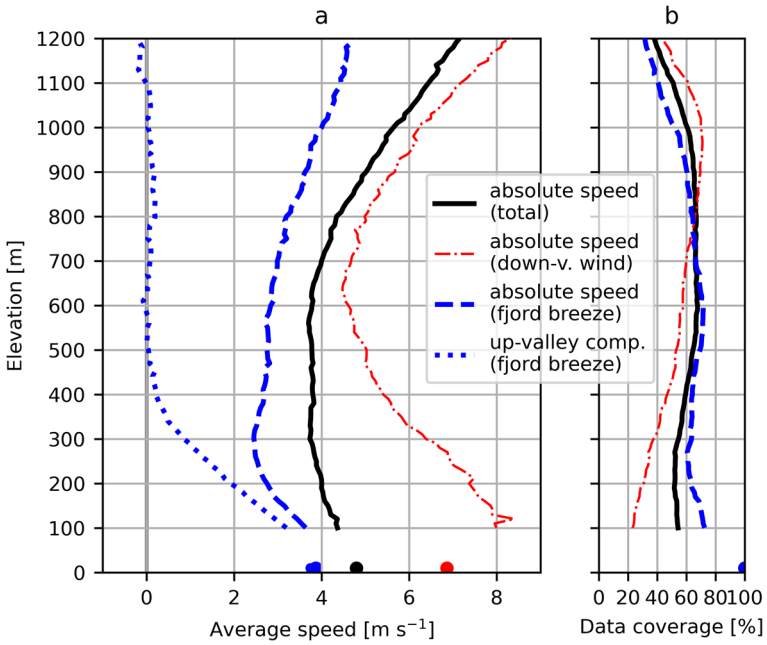

Fig. 8 **a** Average wind speed profiles at V4 based on DBS data, including all profiles (total), only down-valley (at 10 m) profiles, or when the fjord breeze was present at V4. For the last the up-valley component is included in addition to the absolute wind speed. **b** The corresponding data availability by elevation level for the different groups over the period the Lidar was running

Figure 9 gives a picture over the whole campaign period as it portrays the time-series of daily average R_{net} and its range, R_{net}^{SW} and R_{net}^{LW}, as well as days on which a fjord breeze occurred and days on which the large-scale wind was mostly up-valley. Whether or not the fjord breeze occurred on a given day, had little connection to the exact value of R_{net}, since both days with and without a fjord breeze could have high average $R_{net} > 100\,\mathrm{W\,m^{-2}}$ or low average $R_{net} < 50\,\mathrm{W\,m^{-2}}$ values. Instead, it should be noted that R_{net} was positive throughout large parts of each day, generating the local thermal forcing for the fjord breeze. Although the thermal forcing was always in favour of the fjord breeze development, the fjord breeze could be inhibited by strong large-scale down-valley winds. Therefore, it was possible to have days with clear sky, hence strong thermal forcing, but no fjord breeze due to large-scale down-valley winds.

By contrast, the fjord breeze could develop even in cloudy conditions with low thermal forcing when there was no large-scale down-valley wind. However, the large-scale wind sometimes also supported the fjord breeze (Sect. 3.4). Such days with mostly large-scale up-valley wind are marked with red diamonds in Fig. 9, but their proportion was small (19 %).

4 Discussion and Conclusion

The fjord breeze, i.e., a combination of sea breeze and valley wind, was investigated in the High-Arctic archipelago Svalbard. It has been shown that, while normal sea breezes and valley winds have clear diurnal reversals, the fjord breeze can persist over several days and

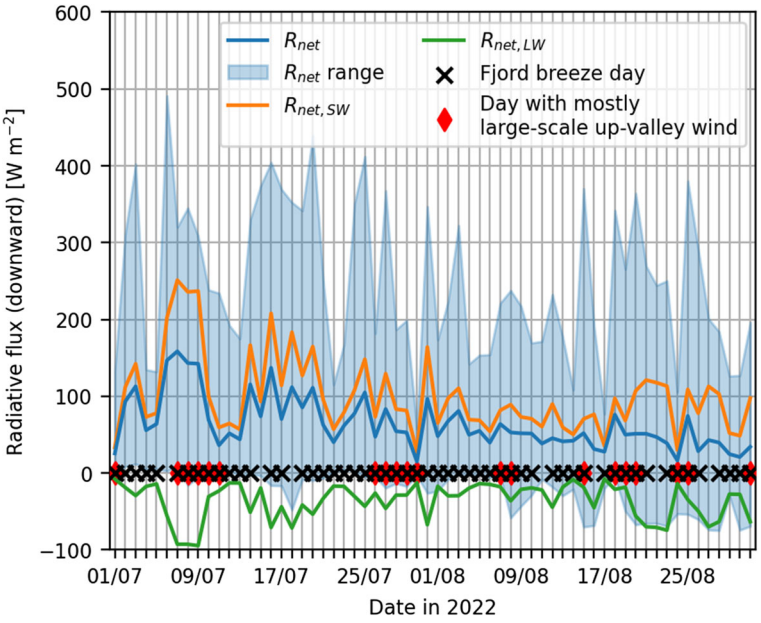

Fig. 9 Average daily radiation values at V4 as well as fjord breeze days and days with mostly large-scale up-valley wind (up-valley at V5 at least 50 % of the time)

cover an extensive area. For Svalbard, where wind energy is currently being investigated as a possible source of energy in the future, these types of local wind phenomena can prove to be very important for the understanding of how much energy can be extracted from the wind and what controls production. It is especially important as the strongest speed-up effect was seen up to 100 m (Fig. 8). Above this height, the wind can decrease, which means that the fjord breeze covers the normal height of modern wind turbines. With the ongoing warming in the Arctic and the continuously reduced snow cover period in Adventdalen (Adakudlu et al. 2019), the fjord breeze will likely become even more important in spring and early summer, since snow cover effectively reduces the heating of the valley by solar radiation.

The fjord breeze was very frequent in the observation period (89 % of the days), and its median daily maximum speed was 5.4 m s^{-1} at V4 (Sect. 3.1). The fjord breeze is comparable to the combined lake-valley wind Ora del Garda in Northern Italy. The Ora del Garda develops in a U-shaped valley, of which the outer part is covered by a large lake. The breeze arrives a few hours after sunrise at the shoreline and continues up-valley, reaching a median speed of 5 m s^{-1} (at 5 m height) and on 70 % of the days in summer (Giovannini et al. 2015). These values compare well to the fjord breeze, although a direct comparison is difficult since the detection of the Ora del Garda is based on a diurnal wind reversal. Giovannini et al. (2015) suspect the additional effect of the valley strengthen the breeze as it is unusually strong and frequent for a normal lake breeze. As the fjord breeze is even more frequent and similarly strong as the Ora del Garda, this suggests that the fjord breeze can be considered unusually strong as well.

The breeze in the Central Valley of California, where large-scale storms are rare in summer, is stronger (over 10 m s^{-1} in some locations) and prevails throughout summer even at night due to the persistent temperature contrast between sea and land. Zhong et al. (2004) found that the up-valley flow is 800 to 1000 m deep, with a maximum speed in the lowest 300 m.

This is larger than the fjord breeze's vertical extent, which, even though it varied depending on the thermal forcing and the large-scale wind (e.g., Fig. 6), had a strong effect only in the lowest 400 m (Fig. 8). The larger speed and depth of this flow compared to the fjord breeze is probably caused by the larger size of the Central Valley (100 s of km) and its surrounding mountains (many peaks between 1000 and 4000 m). The strong persistence of the breeze in the Central Valley is probably due to the absence of large-scale storms, whereas in Adventdalen the fjord breeze is strongly affected by large-scale winds, e.g., strong down-valley winds inhibit the development of the fjord breeze. This explains why the fjord breeze did not occur every day despite the persistent up-valley thermal forcing. The Ora del Garda was found to be affected by large-scale weather in a similar way, e.g. onshore wind led to a stronger breeze and offshore wind could inhibit the breeze (Giovannini et al. 2015).

Moreover, the effect of large-sale down-valley winds on the fjord breeze can be seen in the vertical evolution. The fjord breeze is forced to retreat by large-scale down-valley winds only, starting at the top and propagating downwards (Figs. 3c, 5a). In contrast, classical valley winds like in the Rhone valley (Swiss Alps) change their direction due to the reversal of the thermal forcing, propagating the wind reversal from the surface upwards (Schmid et al. 2020). This illustrates the fundamental difference between the forcing of the Arctic fjord breeze and classical valley winds.

As the fjord breeze extends vertically only to approximately half of the surrounding crest height, it is shallow compared to classical valley winds, e.g., in the Inn and Wipp valley (Austrian Alps) extending roughly 1500 m to crest height (Vergeiner and Dreiseitl 1987; Rucker et al. 2008) or even more than 2500 m in the Rhone valley (Schmid et al. 2020). While this can be partly due to the influence of down-valley winds at higher levels, another reason is likely the advection of cold marine air (Fig. 4b), which leads to an inversion at the top of the fjord breeze, preventing vertical mixing and hence limiting the breeze's vertical extent (e.g., Khodayar et al. 2008). Other studies with similar topographies have found increasing depths of valley winds with distance from the coast, along with a transition from stable to more neutral stratification (e.g., Zhong et al. 2004; Khodayar et al. 2008). This has yet to be shown for the fjord breeze in Adventdalen.

Compared to a normal sea breeze, the fjord breeze is strengthened by the surrounding mountains probably not only through topographic amplification, but also through their shielding effect (Schmidli and Rotunno 2012). Additionally, plateaus, such as the ones south of Adventdalen, are known for increasing the strength of valley winds (Schmidli and Rotunno 2012).

The three case studies (Secs. 3.2, 3.3, 3.4) have illustrated that the development of the fjord breeze is coupled to the local pressure gradient, the heating of the air by the irradiated ground and R_{net}, which strengthens the hypothesis that the fjord breeze in Adventdalen is thermally-driven. In addition, the diurnal variation of the radiative forcing, in combination with the large scale forcing, controls the speed and depth (e.g., Fig. 6) and extent (Fig. 7) of the fjord breeze. While the qualitative connection of the ground heating the air is clear, the numbers are more uncertain as there are great differences between the vertical temperature gradient calculated closest to the ground and between two AWS levels (Fig. 4c). The small gradient at the AWS will inevitably lead to very small fluxes, which can be questioned as elaborated further in Sjöblom (2014) and Sjöblom et al. (2020).

The horizontal temperature gradient can, in addition to the local pressure gradient, be used to quantify the thermal forcing. As an example, the horizontal temperature contrast was ca. 3 °C on 02 August (Fig. 4b). Kozo (1982) found that the temperature difference between the ice-covered sea and bare land on the flat Alaskan north coast was 12 to 14 °C, which led to a sea breeze of similar strength as the fjord breeze (no averages provided by Kozo (1982),

but Fig. 16 therein provides examples of 4 to 7 m s^{-1}). Since the temperature contrast was many times larger in Alaska, one would expect a weaker sea breeze in Adventdalen than in Alaska. Hence, the topography of Adventdalen is probably the factor which compensates for the smaller temperature contrast and strengthens the fjord breeze.

The topography of Adventdalen also influences the interaction of the fjord breeze with other winds, which are mostly channelled through the valley (Fig. 2). Apart from large-scale up-valley winds, large-scale NE-geostrophic winds can also lead to up-valley winds that could be mistaken for a fjord breeze, since the associated pressure gradient forces the wind up-valley, while the NE wind at higher altitudes is channelled down-valley by inner Adventdalen (Fig. 1c). However, these situations probably have minor relevance: In strong NE-geostrophic winds the wind in Adventdalen would be down-valley only. In lighter NE-geostrophic winds, the large-scale pressure gradient is much smaller than the local thermal pressure gradient (e.g., 0.7 vs. 2.3 Pa km^{-1}, Sect. 3.4). The strength of the fjord breeze forcing (maxima of 2 to 4 Pa km^{-1} in the case studies) is in turn very similar to thermal pressure gradients observed in large valleys, e.g., 1.6 Pa km^{-1} (six-day average) in the Inn valley (Vergeiner and Dreiseitl 1987), 2.1 Pa km^{-1} (four-month average) at the entry of the Central Valley (Zhong et al. 2004), and 12 Pa km^{-1} (on one day) in the Elqui Valley (Khodayar et al. 2008).

Although the combination of a sea breeze and valley wind in lower latitudes has been addressed previously, the role of valleys has received little attention in the Arctic. As examples, Esau and Repina (2012) attributed the wintertime down-valley winds in Kongsfjorden, Svalbard, mostly to the land-sea temperature contrast and only secondly to thermal downslope flows, but they did not include the whole valley topography. The numerical studies of Arctic sea breezes by Grønås and Sandvik (1998) also included a large mountain, but no valleys. However, the characteristics of the fjord breeze, the Ora des Garda, and the Central Valley breeze, especially their relatively high frequency and strength, support, together with simulations (Schmidli and Rotunno 2012), that fjord-valley topographies are crucial for the development of the fjord breeze, and their effect should be considered in mountainous parts of the Arctic as well.

To conclude, the fjord breeze is a meteorological phenomenon with high relevance in large Arctic valleys due to its relatively large strength and frequency. Some of the characteristics of the fjord breeze could be attributed to the weak diurnal cycle of radiative forcing, while others are related to the topographic setting. As the fjord breeze is an integral part of the wind climate in Arctic complex terrain, it is important for renewable energy considerations in the Arctic as well, with a possibly large influence on the wind power potential or vertical wind profile in the lowest part of the valley, covering the range of modern wind turbines.

Acknowledgements The authors would like to thank especially Sebastian Sikora for the preparation of the temporary automatic weather stations (AWSs), Arthur Garreau for the extensive support during fieldwork, and Steve Coulson for comments on the manuscript. Moreover, they are grateful for the provision of the Lidar by Joachim Reuder and of one AWS by Marius Jonassen, and for the fieldwork support from various students and staff at UNIS. Hersbach et al. (2018) was downloaded from the Copernicus Climate Change Service (C3S) Climate Data Store. The results contain modified Copernicus Climate Change Service information 2022. Neither the European Commission nor ECMWF is responsible for any use that may be made of the Copernicus information or data it contains. A part of the AWS data was downloaded from MET Norway (2023) and The University Centre in Svalbard (2022). The Lidar used in this study is part of the National Norwegian Research Infrastructure OBLO (Offshore Boundary Layer Observatory (OBLO) funded by the Research Council of Norway (RCN) (project number: 227777). The fieldwork was partly funded by the RCN through an Arctic Field Grant (project number: 333200. RIS ID: 11839).

Funding Open access funding provided by The University Centre in Svalbard

Open Access This article is licensed under a Creative Commons Attribution 4.0 International License, which permits use, sharing, adaptation, distribution and reproduction in any medium or format, as long as you give appropriate credit to the original author(s) and the source, provide a link to the Creative Commons licence, and indicate if changes were made. The images or other third party material in this article are included in the article's Creative Commons licence, unless indicated otherwise in a credit line to the material. If material is not included in the article's Creative Commons licence and your intended use is not permitted by statutory regulation or exceeds the permitted use, you will need to obtain permission directly from the copyright holder. To view a copy of this licence, visit http://creativecommons.org/licenses/by/4.0/.

References

Adakudlu M, Andresen J, Bakke J, Beldring S, Benestad R, Wvd Bilt, Bogen J, Borstad CP, Breili K, Breivik Ø, Børsheim KY, Christiansen HH, Dobler A, Engeset R, Frauenfelder R, Gerland S, Gjelten HM, Gundersen J, Isaksen K, Jaedicke C, Kierulf H, Kohler J, Li H, Lutz J, Melvold K, Mezghani A, Nilsen F, Nilsen IB, Nilsen JEØ, Pavlova O, Ravndal O, Risebrobakken B, Saloranta T, Sandven S, Schuler T, Simpson MJR, Skogen MD, Smedsrud LH, Sund M, Vikhamar-Schuler D, Westermann S, Wong WK (2019) Climate in Svalbard 2100. The Norwegian Centre for Climate Services, Tech rep

Barstad I, Adakudlu M (2011) Observation and modelling of gap flow and wake formation on Svalbard: gap flow and wake formation on Svalbard. Q J R Meteorol Soc 137(660):1731–1738. https://doi.org/10.1002/qj.782

Beine HJ, Argentini S, Maurizi A, Viola A, Mastrantonio G (2001) The local wind field at Ny-Ålesund and the Zeppelin mountain at Svalbard. Meteorol Atmos Phys 78(1–2):107–113. https://doi.org/10.1007/s007030170009

Bromwich DH, Du Y, Hines KM (1996) Wintertime Surface Winds over the Greenland Ice Sheet. Mon Weather Rev 124(9):1941–1947. https://doi.org/10.1175/1520-0493(1996)124<1941:WSWOTG>2.0.CO;2

Cheynet E, Flügge M, Reuder J, Jakobsen JB, Heggelund Y, Svardal B, Saavedra Garfias P, Obhrai C, Daniotti N, Berge J, Duscha C, Wildmann N, Onarheim IH, Godvik M (2021) The COTUR project: remote sensing of offshore turbulence for wind energy application. Atmos Meas Tech 14(9):6137–6157. https://doi.org/10.5194/amt-14-6137-2021

Cisek M, Petelski T, Zielinski T, Makuch P, Pakszys P, Rozwadowska A, Markuszewski P (2017) Aerosol optical depth variations due to local breeze circulation in Kongsfjorden, Spitsbergen. Oceanologia 59(4):422–430. https://doi.org/10.1016/j.oceano.2017.04.005

Claremar B, Obleitner F, Reijmer C, Pohjola V, Waxegård A, Karner F, Rutgersson A (2012) Applying a mesoscale atmospheric model to Svalbard glaciers. Adv Meteorol 2012:1–22. https://doi.org/10.1155/2012/321649

de Witt M, Stefánsson H, Valfells A, Larsen JN (2021) Energy resources and electricity generation in Arctic areas. Renew Energy 169:144–156. https://doi.org/10.1016/j.renene.2021.01.025

Doran PT, McKay CP, Clow GD, Dana GL, Fountain AG, Nylen T, Lyons WB (2002) Valley floor climate observations from the McMurdo dry valleys, Antarctica, 1986–2000. J Geophys Res Atmos 107(D24). https://doi.org/10.1029/2001JD002045

Esau I, Repina I (2012) Wind climate in Kongsfjorden, Svalbard, and attribution of leading wind driving mechanisms through turbulence-resolving simulations. Adv Meteorol 2012:1–16. https://doi.org/10.1155/2012/568454

Gallée H, Duynkerke PG (1997) Air-snow interactions and the surface energy and mass balance over the melting zone of west Greenland during the Greenland Ice Margin Experiment. J Geophys Res Atmos 102(D12):13,813-13,824. https://doi.org/10.1029/96JD03358

Giovannini L, Laiti L, Zardi D, de Franceschi M (2015) Climatological characteristics of the Ora del Garda wind in the Alps: climatological characteristics of the Ora del Garda wind in the Alps. Int J Climatol 35(14):4103–4115. https://doi.org/10.1002/joc.4270

Grønås S, Sandvik AD (1998) Numerical simulations of sea and land breezes at high latitudes. Tellus A Dyn Meteorol Oceanogr 50(4):468–489. https://doi.org/10.3402/tellusa.v50i4.14539

Henkies M, Duscha C, Reuder J, Sjöblom A (2023a) Wind Lidar Measurements in Adventdalen, Svalbard, 2022. https://doi.org/10.21343/MFNG-6727

Henkies M, Sikora S, Sjöblom A (2023b) Meteorological near-surface observations in the area of Adventdalen, Svalbard, in summer 2022. https://doi.org/10.21343/TSVH-Y187

Hersbach H, Bell B, Berrisford P, Biavati G, Horányi A, Muñoz Sabater J, Nicolas J, Peuby C, Radu R, Rozum I, Schepers D, Simmons A, Soci C, Dee D, Thépaut JN (2018) ERA5 hourly data on pressure levels from 1959 to present. https://doi.org/10.24381/cds.adbb2d47

Jung T, Gordon ND, Bauer P, Bromwich DH, Chevallier M, Day JJ, Dawson J, Doblas-Reyes F, Fairall C, Goessling HF, Holland M, Inoue J, Iversen T, Klebe S, Lemke P, Losch M, Makshtas A, Mills B, Nurmi P, Perovich D, Reid P, Renfrew IA, Smith G, Svensson G, Tolstykh M, Yang Q (2016) Advancing polar prediction capabilities on daily to seasonal time scales. Bull Am Meteorol Soc 97(9):1631–1647. https://doi.org/10.1175/BAMS-D-14-00246.1

Kalthoff N, Bischoff-Gauß I, Fiebig-Wittmaack M, Fiedler F, Thürauf J, Novoa E, Pizarro C, Castillo R, Gallardo L, Rondanelli R, Kohler M (2002) Mesoscale Wind Regimes in Chile at 30°S. J Appl Meteorol 41(9):953–970. https://doi.org/10.1175/1520-0450(2002)041<0953:MWRICA>2.0.CO;2

Khodayar S, Kalthoff N, Fiebig-Wittmaack M, Kohler M (2008) Evolution of the atmospheric boundary-layer structure of an arid Andes Valley. Meteorol Atmos Phys 99(3–4):181–198. https://doi.org/10.1007/s00703-007-0274-3

Kilpeläinen T, Vihma T, Ólafsson H (2011) Modelling of spatial variability and topographic effects over Arctic fjords in Svalbard. Tellus A Dyn Meteorol Oceanogr 63(2):223. https://doi.org/10.1111/j.1600-0870.2010.00481.x

Kilpeläinen T, Vihma T, Manninen M, Sjöblom A, Jakobson E, Palo T, Maturilli M (2012) Modelling the vertical structure of the atmospheric boundary layer over Arctic fjords in Svalbard: atmospheric boundary layer over arctic fjords. Q J R Meteorol Soc 138(668):1867–1883. https://doi.org/10.1002/qj.1914

Kitowska M, Petelski T (2021) Svalbard's mesoscale environmental factor impact on the wind field. Atmosphere 12(9):1165. https://doi.org/10.3390/atmos12091165

Kitowska M, Makuch P, Petelski T, Piskozub J (2021) The influence of mesoscale land-sea breeze circulation on local wind climatology in the Svalbard fjords of Kongsfjorden and Hornsund. Int J Climatol 41(S1). https://doi.org/10.1002/joc.6731

Kondo H (1990) A numerical experiment on the interaction between Sea Breeze and Valley wind to generate the so-called "Extended Sea Breeze". J Meteorol Soc Jpn 68(4):435–446. https://doi.org/10.2151/jmsj1965.68.4_435

Kozo TL (1982) An observational study of sea breezes along the Alaskan Beaufort sea coast: part I. J Appl Meteorol 21(7):891–905. https://doi.org/10.1175/1520-0450(1982)021<0891:AOSOSB>2.0.CO;2

Leopold LB (1949) The interaction of trade wind and sea Breeze, Hawaii. J Meteorol 6(5):312–320. https://doi.org/10.1175/1520-0469(1949)006<0312:TIOTWA>2.0.CO;2

Mahrer Y, Pielke RA (1977) The effects of topography on sea and land breezes in a two-dimensional numerical model. Mon Weather Rev 105(9):1151–1162. https://doi.org/10.1175/1520-0493(1977)105<1151:TEOTOS>2.0.CO;2

Mäkiranta E, Vihma T, Sjöblom A, Tastula EM (2011) Observations and modelling of the atmospheric boundary layer over sea-ice in a Svalbard fjord. Boundary-Layer Meteorol 140(1):105–123. https://doi.org/10.1007/s10546-011-9609-1

Mayer S, Jonassen MO, Sandvik A, Reuder J (2012) Profiling the arctic stable boundary layer in advent valley, Svalbard: measurements and simulations. Boundary-Layer Meteorol 143(3):507–526. https://doi.org/10.1007/s10546-012-9709-6

Mazon J, Rojas JI, Jou J, Valle A, Olmeda D, Sanchez C (2015) An assessment of the sea breeze energy potential using small wind turbines in peri-urban coastal areas. J Wind Eng Ind Aerodyn 139:1–7. https://doi.org/10.1016/j.jweia.2015.01.002

McKendry IG, Lewthwaite EWD (1992) Summertime along-valley wind variations in the wright valley Antarctica. Int J Climatol 12(6):587–596. https://doi.org/10.1002/joc.3370120605

MET Norway (2022) Frost API. https://frost.met.no/dataclarifications.html

MET Norway (2023) Meteorological data. frost.met.no

Miller GH, Alley RB, Brigham-Grette J, Fitzpatrick JJ, Polyak L, Serreze MC, White JW (2010) Arctic amplification: can the past constrain the future? Quat Sci Rev 29(15–16):1779–1790. https://doi.org/10.1016/j.quascirev.2010.02.008

Moritz RE, Bitz CM, Steig EJ (2002) Dynamics of recent climate change in the arctic. Science 297(5586):1497–1502. https://doi.org/10.1126/science.1076522

Nylen TH, Fountain AG, Doran PT (2004) Climatology of katabatic winds in the McMurdo dry valleys, southern Victoria Land, Antarctica. J Geophys Res Atmos 109(D03114). https://doi.org/10.1029/2003JD003937

Oerlemans J, Vugts HF (1993) A meteorological experiment in the melting zone of the Greenland Ice sheet. Bull Am Meteor Soc 74(3):355–365. https://doi.org/10.1175/1520-0477(1993)074<0355:AMEITM>2.0.CO;2

Parish TR, Bromwich DH (2007) Reexamination of the near-surface airflow over the antarctic continent and implications on atmospheric circulations at high southern latitudes. Mon Weather Rev 135(5):1961–1973. https://doi.org/10.1175/MWR3374.1

Previdi M, Smith KL, Polvani LM (2021) Arctic amplification of climate change: a review of underlying mechanisms. Environ Res Lett 16(9):093,003. https://doi.org/10.1088/1748-9326/ac1c29
Radu D, Berger M, Fonteneau R, Hardy S, Fettweis X, Le Du M, Panciatici P, Balea L, Ernst D (2019) Complementarity assessment of south Greenland katabatic flows and West Europe wind regimes. Energy 175:393–401. https://doi.org/10.1016/j.energy.2019.03.048
Richner H, Hächler P (2013) Understanding and Forecasting Alpine Foehn. In: Chow FK, De Wekker SF, Snyder BJ (eds) Mountain weather research and forecasting: recent progress and current challenges. Springer, New York
Rucker M, Banta RM, Steyn DG (2008) Along-valley structure of daytime thermally driven flows in the Wipp valley. J Appl Meteorol Clim 47(3):733–751. https://doi.org/10.1175/2007JAMC1319.1
Sandvik AD, Furevik BR (2002) Case study of a coastal jet at Spitsbergen-comparison of SAR- and model-estimated wind. Mon Weather Rev 130(4):1040–1051. https://doi.org/10.1175/1520-0493(2002)130<1040:CSOACJ>2.0.CO;2
Schmid F, Schmidli J, Hervo M, Haefele A (2020) Diurnal valley winds in a deep alpine valley: observations. Atmosphere 11(1):54. https://doi.org/10.3390/atmos11010054
Schmidli J, Rotunno R (2012) Influence of the valley surroundings on valley wind dynamics. J Atmos Sci 69(2):561–577. https://doi.org/10.1175/JAS-D-11-0129.1
Schön M, Suomi I, Altstädter B, van Kesteren B, zum Berge K, Platis A, Wehner B, Lampert A, Bange J (2022) Case studies of the wind field around Ny-Ålesund, Svalbard, using unmanned aircraft. Polar Res 41:7884, https://doi.org/10.33265/polar.v41.7884
Serreze MC, Barry RG (2011) Processes and impacts of Arctic amplification: a research synthesis. Glob Planet Change 77(1–2):85–96. https://doi.org/10.1016/j.gloplacha.2011.03.004
Shestakova AA, Chechin DG, Lüpkes C, Hartmann J, Maturilli M (2022) The foehn effect during easterly flow over Svalbard. Atmos Chem Phys 22(2):1529–1548. https://doi.org/10.5194/acp-22-1529-2022
Sjöblom A (2014) Turbulent fluxes of momentum and heat over land in the high-arctic summer: the influence of observation techniques. Polar Res 33(1):21,567. https://doi.org/10.3402/polar.v33.21567
Sjöblom A, Andersson A, Rutgersson A, Falck E (2020) Flow over a snow-water-snow surface in the high Arctic, Svalbard: turbulent fluxes and comparison of observation techniques. Polar Sci 25(100):549. https://doi.org/10.1016/j.polar.2020.100549
Skeie P, Grønås S (2000) Strongly stratified easterly flows across Spitsbergen. Tellus A Dyn Meteorol Oceanogr 52(5):473. https://doi.org/10.3402/tellusa.v52i5.12281
Steele CJ, Dorling SR, von Glasow R, Bacon J (2015) Modelling sea-breeze climatologies and interactions on coasts in the southern North Sea: implications for offshore wind energy: Sea-Breeze types and characteristics offshore. Q J R Meteorol Soc 141(690):1821–1835. https://doi.org/10.1002/qj.2484
The University Centre in Svalbard (2022) Weather stations. https://www.unis.no/facilities/weather-stations/
Valkonen T, Stoll P, Batrak Y, Køltzow M, Schneider TM, Stigter EE, Aashamar OB, Støylen E, Jonassen MO (2020) Evaluation of a sub-kilometre NWP system in an Arctic fjord-valley system in winter. Tellus A Dyn Meteorol Oceanogr 72(1):183,. https://doi.org/10.1080/16000870.2020.1838181
Van Den Broeke MR, Van Lipzig NPM (2003) Factors controlling the near-surface wind field in Antarctica. Mon Weather Rev 131(4):733–743. https://doi.org/10.1175/1520-0493(2003)131<0733:FCTNSW>2.0.CO;2
Vergeiner I, Dreiseitl E (1987) Valley winds and slope winds. Observations and elementary thoughts. Meteorol Atmos Phys 36(1–4):264–286. https://doi.org/10.1007/BF01045154
Vihma T, Kilpeläinen T, Manninen M, Sjöblom A, Jakobson E, Palo T, Jaagus J, Maturilli M (2011) Characteristics of temperature and humidity inversions and low-level jets over Svalbard fjords in spring. Adv Meteorol 2011:1–14. https://doi.org/10.1155/2011/486807
Whiteman CD, Doran JC (1993) The relationship between overlying synoptic-scale flows and winds within a valley. J Appl Meteorol 32(11):1669–1682. https://doi.org/10.1175/1520-0450(1993)032<1669:TRBOSS>2.0.CO;2
Xia G, Draxl C, Optis M, Redfern S (2022) Detecting and characterizing simulated sea breezes over the US northeastern coast with implications for offshore wind energy. Wind Energy Sci 7(2):815–829. https://doi.org/10.5194/wes-7-815-2022
Zardi D, Whiteman CD (2013) Diurnal mountain wind systems. In: Chow FK, De Wekker SF, Snyder BJ (eds) Mountain weather research and forecasting. Springer, Netherlands
Zhang J, Liu F, Tao W, Krieger J, Shulski M, Zhang X (2016) Mesoscale climatology and variation of surface winds over the Chukchi–Beaufort coastal areas. J Clim 29(8):2721–2739. https://doi.org/10.1175/JCLI-D-15-0436.1
Zhong S, Whiteman CD, Bian X (2004) Diurnal evolution of three-dimensional wind and temperature structure in California's Central Valley. J Appl Meteorol 43(11):1679–1699. https://doi.org/10.1175/JAM2154.1

Publisher's Note Springer Nature remains neutral with regard to jurisdictional claims in published maps and institutional affiliations.